

8C.2

DOUBLE WARM-CORE STRUCTURE OF TYPHOON LAN (2017) AS OBSERVED THROUGH UPPER-TROPOSPHERIC AIRCRAFT RECONNAISSANCE DURING T-PARCII

Hiroyuki Yamada¹, Kazuhisa Tsuboki², Norio Nagahama³, Kensaku Shimizu³, Tadayasu Ohigashi⁴, Taro Shinoda², Kosuke Ito¹, Munehiko Yamaguchi⁵, and Tetsuo Nakazawa⁵

1: University of the Ryukyus, Okinawa, Japan, 2: Nagoya University, Nagoya, Japan, 3: Meisei Electric, Isesaki, Japan, 4: National Research Institute for Earth Science and Disaster Resilience, Tsukuba, Japan, 5: Meteorological Research Institute, Tsukuba, Japan

1. INTRODUCTION

In the western North Pacific, since aircraft reconnaissance by the US military ceased in 1987, the central pressure of a typhoon has not been observed for approximately 30 years, except for several special field experiments. In the Japan Meteorological Agency (JMA), typhoon intensity is estimated using geostationary satellite imagery and microwave sensors (Oyama et al. 2016). In recent years, ground-based Doppler radars are also used experimentally to estimate intensity (Shimada et al. 2016). However, the problem remains that these intensity estimates are not verified by direct observation in this basin. The Tropical Cyclones-Pacific Asian Research Campaign for the Improvement of Intensity Estimations/Forecasts (T-PARCII) has been funded for the period from 2016 through 2020 as a Grant-in-Aid for Scientific Research (S) by the Japan Society for the Promotion of Science. On 21–22 October 2017, the first reconnaissance mission was flown for Typhoon Lan with Category-4 intensity. This flight was made using a Gulfstream-II jet aircraft with a GPS dropsounding system newly developed by Meisei Electric (Fig. 1). We selected an upper-tropospheric flight level of 43,000 ft (~13.8 km) for



Fig. 1 Photographs of (a) the Gulfstream-II jet and (b) a Meisei iMDS-17 dropsonde.

collecting sounding data in as deep a layer as possible. By gazing at the display of the aviation weather radar and selecting a path in an area of weak precipitation echo of the eyewall, we succeeded in flying into the eye three times without suffering severe turbulence. In this paper, we describe the double warm-core structure and visible features of the eye and eyewall using dropsonde data and photographs during the flight mission. In the analyses, the center position of the typhoon was identified every 2.5 minutes by using Himawari-8 rapid-scan infrared imagery. The center was defined as the centroid of the shallow-cloud area (< 5 km MSL) inside the eyewall.

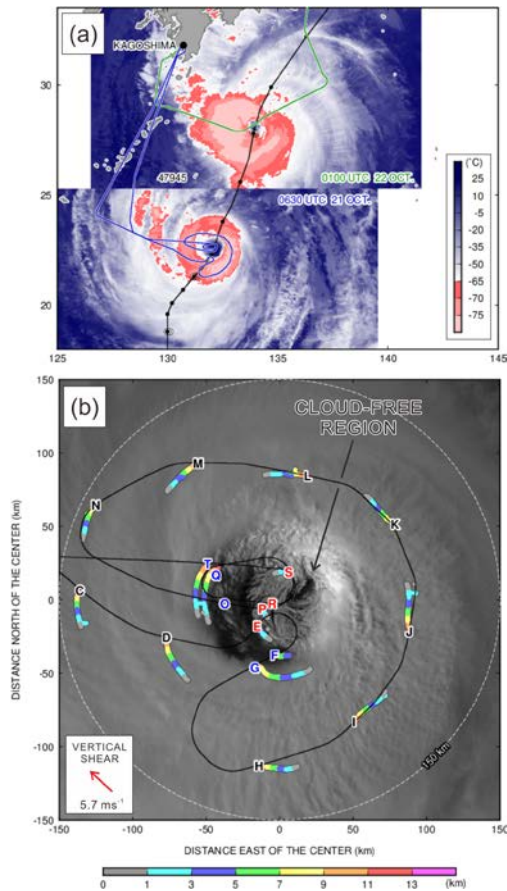


Fig. 2 (a) Infrared brightness temperature distributions and flight path on 21 (blue) and 22 (green) October 2017. Best track position is plotted every 6 hours. (b) Position and altitude of dropsondes relative to the typhoon center during the flight mission on 21 October. A white broken circle indicates a 150-km radius from the center.

2. OVERVIEW OF RECONNAISSANCE

The flights into the inner-core region were made from 0500 through 0700 UTC on 21 October and around 0100 UTC on the next day (Fig. 2a). According to the best track records of Japan Meteorological Agency (JMA) and Joint Typhoon Warning Center, this typhoon was almost in the mature phase of Saffir-Simpson Category-4 intensity, with a minimum central pressure of 915–935 hPa. The minimum surface pressure in our

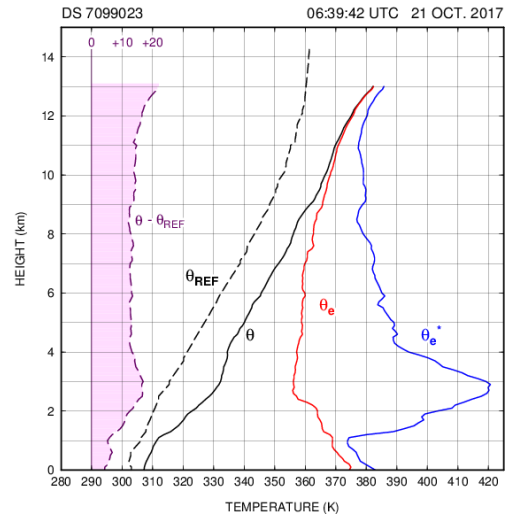


Fig. 3 Vertical profiles of potential temperature (θ), equivalent potential temperature (θ_e), saturated equivalent potential temperature (θ_e^*), potential temperature of the reference profile (θ_{REF}), and potential temperature anomaly ($\theta - \theta_{REF}$) near the typhoon center, deployed at the position “R” in Fig. 2b at 0639 UTC on 21 October.

observation was 925 hPa, obtained by the dropsonde labeled “R” in Fig. 2b. A large eye with a diameter of 90 km, well-established concentric eyewall convection, and inactive outer rainbands during the flight on the first day are characteristics of an annular typhoon (Knaff et al. 2003; Chu and Tan 2014). At that time, the environmental vertical shear between 850 and 200 hPa within the annuli between 200 and 800 km, calculated using the JRA-55 reanalysis dataset, was 5.7 m s^{-1} toward northwest. The flight route on this day was initially designed to circumnavigate the eyewall within the 200 km radius; however, the route was eventually modified to go into the eye. This decision was made with pilots in flight using a display of the aviation weather radar that showed “green” (representing light precipitation) in a part of eyewall convection at the flight level. During the two flights, 4, 5, and 17

dropsondes were deployed in the eye, eyewall, and surrounding region, respectively (Fig. 2b). The deployment from the upper troposphere enabled us to examine the thermodynamic features of the eye in the lower and middle troposphere and, marginally, in the upper troposphere.

3. DOUBLE WARM-CORE STRUCTURE

The vertical profile of a sounding deployed close to the circulation center at 0639 UTC on 21 October is shown in Fig. 3. The anomaly of potential temperature ($\theta - \theta_{\text{REF}}$) was determined using a local reference sounding obtained at 0600 UTC at the JMA 47945 (Minamidaitojima) site, which was 400 km north of the eye. The anomaly profile showed positive values extending from the lower through upper troposphere, with two peaks near 3 km (~ 700 hPa) and above 12 km MSL (< 200 hPa). The estimated anomalies were approximately +12 K on average, +16 K at the lower peak, and >20 K at the upper peaks. The magnitude of the anomaly in the upper troposphere was close to that recently observed in major hurricanes (e.g., Doyle et al. 2017), and supports a positive relationship between the strength of the warm core and typhoon intensity, as should be expected for a balanced vortex (Shapiro and Willoughby 1982). In contrast, the altitude of the lower peak was approximately 1–2 km lower than that reported in many of the previous observations (e.g., Hawkins and Imbembo 1976; Halverson et al. 2006; Munsell et al. 2018). The lower-tropospheric warm core was captured not only in the first day but also in the second day (not shown). Another notable feature is an extremely large value of the saturated equivalent potential temperature (θ_e^*) of the low-level warm core,

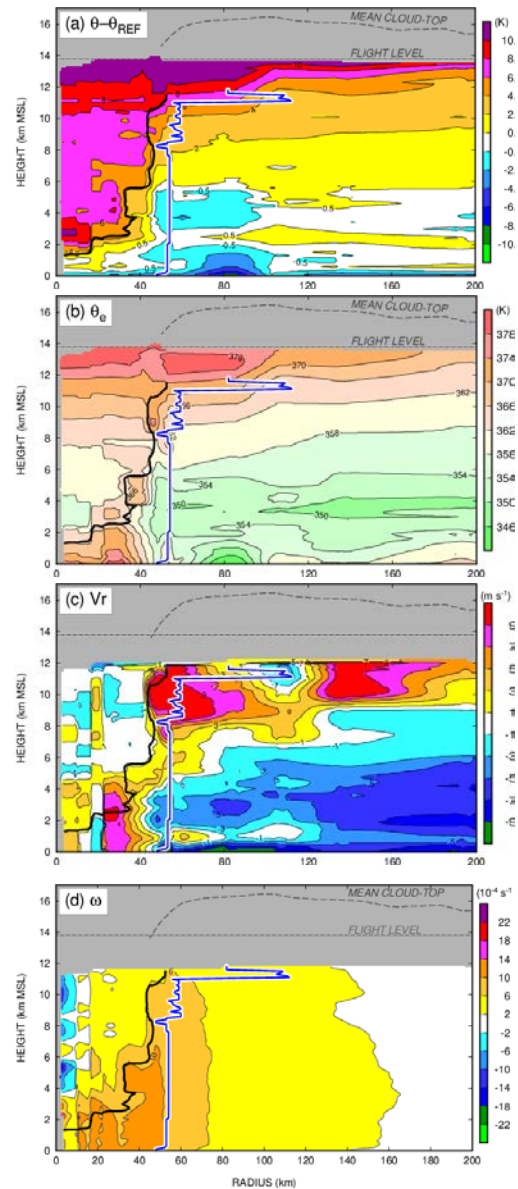


Fig. 4 Radial-height composite plots of (a) potential temperature anomaly, (b) equivalent potential temperature, (c) radial wind component, and (d) angular velocity in 0510–0715 UTC on 21 October. A black line indicates the inner eyewall boundary, defined by using the 70% contour of relative humidity. A blue line indicates the radius of maximum tangential winds (RMW). The mean cloud-top height was estimated using Himawari-8 infrared imagery.

reaching 420 K. The values of θ , θ_e , and θ_e^* at this level can be obtained if the reference profile is adiabatically descended to 2.3 km. This estimation

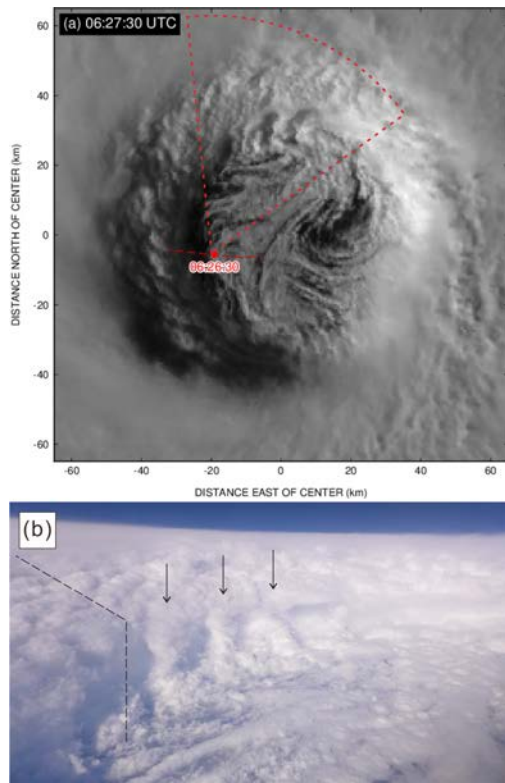


Fig. 5 (a) Himawari-8 rapid-scan visible imagery of the eye at 06:27:30 UTC on 21 October. (b) A photograph of the eyewall boundary taken 1 minutes later. Arrows indicate finger-like features, and a broken line shows the slope of the eyewall boundary. The aircraft position and viewing angle are shown in (a).

suggests dry adiabatic warming within the eye. This supports the hypothesis of Willoughby (1998), in which the air above the eye inversion has remained in the eye since it was enclosed when the eyewall formed and that it has subsided, at most, a few kilometers.

Figure 4 shows the radius-height distribution, plotted using selected dropsondes deployed in the inner core and the western (i.e., downshear-left) side of the outer core. Sounding data were interpolated using the Cressman scheme within 5

km of the horizontal radius and 1 km of the vertical distance. Gaps between the two grids with valid data were linearly interpolated. The distribution of the potential temperature anomaly (Fig. 4a) indicates that the lower-level warm core was concentrated within 15 km of the center, while the eye radius was approximately 45 km. Figure 4b shows the difference in the equivalent potential temperature (θ_e) between the lower-level warm core (< 358 K) and the surrounding area within the eye (> 366 K). Areas of θ_e greater than 366 K were also distributed below the inversion layer of the eye (height less than 2 km) and along the inside eyewall boundary. Since this high- θ_e along the eyewall boundary generally coexisted with outward radial winds (positive V_r in Fig. 4c), this corresponds to updrafts of the tilted eyewall. The existence of high- θ_e in the eye inversion and in the eyewall updraft suggests the transport of air from the eye inversion layer into the eyewall updraft. The distribution of angular velocity (Fig. 4d) shows nearly monotonic distribution within the radius of maximum tangential wind (RMW, a blue line) below 3 km MSL, while a decrease in angular velocity is significant in the eye above 4 km MSL. The value of angular velocity in the eye at 1 km MSL ($\sim 12 \times 10^{-4} \text{ s}^{-1}$) is consistent with the rotating speed of a cloud-free region in the eye (indicated in Fig. 2b), which took approximately 90 minutes per rotation, yielding an angular velocity of $11.6 \times 10^{-4} \text{ s}^{-1}$. Both the monotonic distribution of the angular velocity (i.e., solid-body rotation) in the eye and the existence of high- θ_e in the eye and eyewall updraft suggest the horizontal mixing of air between the eye and eyewall (Kossin and Eastin 2001; Cram et al. 2007; Hazelton et al. 2017). In this sense, the existence of the low-level warm core

with lower θ_e and lower angular velocity above 3 km MSL suggests the isolation of descended air near the eye center above the inversion.

4. VISIBLE FEATURES OF THE EYEWALL

Morphological features of the eyewall boundary, associated with eye-eyewall mixing, are shown by combining a rapid-scan satellite imagery with a photograph (Fig. 5). In the northern part of the eye (Fig. 5a), curved and finger-like cloud features are evident, and they are connected to the eyewall boundary. The view from flight level (Fig. 5b) clearly shows the vertical structure of these features, extending almost vertically to the middle of the whole cloud depth (i.e., ~ 8 km MSL). It is also evident that the slope of the eyewall boundary significantly changed above the finger-like cloud features. Similar features were previously reported in cases of intense hurricanes (e.g., Bluestein and Marks 1987; Aberson et al. 2006; Marks et al. 2008), whereas the characteristics of vertical extent (i.e., depth and uprightness) in the present case are different from those in previous cases. We hypothesized that these finger-like features correspond to mesovortices, possessing strong updrafts and vorticity, and are caused by rising high- θ_e air from the eye inversion layer.

5. SUMMARY AND DISCUSSION

We succeeded in flying into the eye of Typhoon Lan (2017) with Category-4 intensity and in deploying dropsondes from the upper troposphere (13.8 km MSL). The characteristics obtained from the analysis of dropsonde data are:

- double warm-core structure in the large eye with a radius of 45 km during the phase of annular-typhoon structure,

- relatively lower altitude (~ 3 km MSL) of the lower-tropospheric warm core that concentrated within 15 km of the circulation center,
- high- θ_e (> 366 K) air below the eye inversion and in eyewall updrafts,
- monotonic distribution of angular velocity in the eye and eyewall just below the lower-tropospheric warm core, and
- curved and finger-like features of the eyewall inner boundary, suggesting the existence of mesovortices.

These features suggest eye-eyewall mixing below the eye inversion layer and the isolation of descending air near the center of the eye due to a lack of stirring above the inversion. The further intension of this study is to investigate the role of these processes in the eye on the longevity of the peak intensity of annular tropical cyclones (Knaff et al. 2003; Chu and Tan 2014), using a cloud-resolving numerical simulation.

Another point to be noted is that this is the first attempt at upper-tropospheric reconnaissance of the eye of a typhoon in the western North Pacific using a jet aircraft, as proposed 39 years ago by Gray (1979). He argued that, in the upper troposphere, winds are significantly weaker, and turbulence is generally less intense if echoes can be avoided using aviation weather radar. A recent improvement of a the GPS dropsonde system made it possible to capture kinematic and thermodynamic features from the upper to lower troposphere without fatal signal loss. It would also be worth investigating and predicting the occurrence of upper-tropospheric disturbances (such as gravity waves from convective bursts) for

avoiding severe turbulence during upper-tropospheric reconnaissance.

Acknowledgments

The authors express their gratitude to Diamond Air Service Inc. for their support of reconnaissance flights. We especially thank the pilots of the Gulfstream-II jet for their flexibility in flight-route determination inside the typhoon. This work was supported by JSPS KAKENHI Grant Numbers JP16H06311 and JP16H04053. Himawari-8 rapid-scan imagery was provided by Science Cloud of the National Institute of Information and Communications Technology (<http://sc-web.nict.go.jp/SCindex.html>).

References

- Aberson, S. D., M. T. Montgomery, M. Bell, and M. Black, 2006: Hurricane Isabel (2003): New insights into the physics of intense storms. Part II: Extreme localized wind. *Bull. Amer. Meteor. Soc.*, **87**, 1349–1354.
- Bluestein, H. B., and F. D. Marks, 1987: On the structure of the eyewall of Hurricane Diana (1984): Comparison of radar and visual characteristics. *Mon. Wea. Rev.*, **115**, 2542–2552.
- Chu, K. and Z. Tan, 2014: Annular typhoons in the western North Pacific. *Wea. Forecasting*, **29**, 241–251.
- Cram, T. A., J. Persing, M. T. Montgomery, and S. A. Braun, 2007: A Lagrangian trajectory view on transport and mixing processes between the eye, eyewall, and environment using a high-resolution simulation of Hurricane Bonnie (1998). *J. Atmos. Sci.*, **64**, 1835–1856.
- Doyle, J. D. and Coauthors, 2017: A view of tropical cyclones from above: The tropical cyclone intensity experiment. *Bull. Amer. Meteor. Soc.*, **98**, 2113–2134.
- Gray, W. M., 1979: Tropical Cyclone Intensity Determination Through Upper-Tropospheric Aircraft Reconnaissance. *Bull. Amer. Meteor. Soc.*, **60**, 1069–1076.
- Halverson, J. B., J. Simpson, G. Heymsfield, H. Pierce, T. Hock, and L. Ritchie, 2006: Warm core structure of Hurricane Erin diagnosed from high altitude dropsondes during CAMEX-4. *J. Atmos. Sci.*, **63**, 309–324.
- Hawkins, H. F. and S. M. Imbembo, 1976: The structure of a small, intense hurricane—Inez 1966. *Mon. Wea. Rev.*, **104**, 418–442.
- Hazelton, A. T., R. F. Rogers, and R. E. Hart, 2017: Analyzing simulated convective bursts in two Atlantic hurricanes. Part I: Burst formation and development. *Mon. Wea. Rev.*, **145**, 3073–3094.
- Knaff, J. A., J. P. Kossin, and M. DeMaria, 2003: Annular hurricanes. *Wea. Forecasting*, **18**, 204–223.
- Kossin, J. P. and M. D. Eastin, 2001: Two distinct regimes in the kinematic and thermodynamic structure of the hurricane eye and eyewall. *J. Atmos. Sci.*, **58**, 1079–1090.
- Marks, F. D., P. G. Black, M. T. Montgomery, and R. W. Burpee, 2008: Structure of the eye and eyewall of Hurricane Hugo (1989). *Mon. Wea. Rev.*, **136**, 1237–1259.
- Munsell, E. B., F. Zhang, S. A. Braun, J. A. Sippel, and A. C. Didlake, 2018: The Inner-core temperature structure of Hurricane Edouard (2014): Observations and ensemble variability. *Mon. Wea. Rev.*, **146**, 135–155.
- Oyama, R., K. Nagata, H. Kawada, and N. Koide, 2016: Development of a product based on consensus between Dvorak and AMSU tropical cyclone central pressure estimates at JMA. *RSMC Tokyo-Typhoon Center Technical Review*, **18**, (available at <http://www.jma.go.jp/jma/jma-eng/jma-center/rsmc-hp-pub-eg/techrev.htm>).
- Shapiro, L. J., and H. E. Willoughby, 1982: The response of balanced hurricanes to local sources of heat and momentum. *J. Atmos. Sci.*, **39**, 378–394.
- Shimada, U., M. Sawada, and H. Yamada, 2016: Evaluation of the accuracy and utility of tropical cyclone intensity estimation using single ground-based Doppler radar observations. *Mon. Wea. Rev.*, **144**, 1823–1840.
- Willoughby, H. E., 1998: Tropical cyclone eye thermodynamics. *Mon. Wea. Rev.*, **126**, 3053–3067.